Journal of Molecular Liquids 355 (2022) 118955

Contents lists available at ScienceDirect

Journal of Molecular Liquids

journal homepage: www.elsevier.com/locate/molliq

Structure, dynamics and conductivities of ionic liquid-alcohol mixtures

José M. Otero-Mato [a], Hadrián Montes-Campos [a], Víctor Gómez-González [a], Martín Montoto [a], Oscar Cabeza [b], Svyatoslav Kondrat [c,d,e], Luis M. Varela [a,*]

[a] Grupo de Nanomateriais, Fotónica e Materia Branda, Departamento de Física de Partículas, Facultade de Física and Instituto de Materiais (iMATUS), Universidade de Santiago de Compostela, Campus Vida s/n E-15782, Santiago de Compostela, Spain
[b] Facultade de Ciencias, Universidade da Coruña, Campus A Zapateira s/n E-15071, A Coruña, Spain
[c] Institute of Physical Chemistry, Polish Academy of Sciences, Kasprzaka 44/52, 01-224 Warsaw, Poland
[d] Max-Planck-Institut für Intelligente Systeme, Heisenbergstraße 3, 70569 Stuttgart, Germany
[e] IV. Institut für Theoretische Physik, Universität Stuttgart, Pfaffenwaldring 57, 70569 Stuttgart, Germany

ARTICLE INFO

Article history:
Received 16 January 2022
Revised 8 March 2022
Accepted 15 March 2022
Available online 19 March 2022

Keywords:
Ionic liquids
Conductivity
Structure
Alcohols
Molecular dynamics simulation

ABSTRACT

We study the microscopic structure and transport properties of ions in mixtures of 1-butyl-3-methylimidazolium and 1-butyl-3-ethylimidazolium iodide with ethanol using atomistic molecular dynamics simulations and conductivity measurements. Compared with the same ionic liquids in water, we reveal essential differences in ionic structure that are closely related to the differences in the solubility mechanisms of both types of solvents. In particular, unlike for aqueous solutions, we find a homogeneous distribution of solvent molecules in the system, i.e., we observe no cluster formation, which agrees with the nano-structured solvation paradigm. In addition, we calculate the conductivities of these systems in the whole concentration range and compare them with experimental data. Although the simulated values slightly underestimate the experimental ones, they reproduce the shape of the experimental conductivity dome reasonably well. We also show that the pseudo-lattice random-alloy model, which is based on microscopic ion jumping frequencies, describes the conductivity data accurately. We compute the average jumping frequencies directly from simulations and find that they agree well with those obtained by fitting the simulation conductivity data. These results show that the pseudo-lattice random-alloy model provides a valuable tool to describe the conductivities of ionic liquid–solvent mixtures and particularly their concentration dependence. It shall also apply to other systems, e.g., inorganic electrolytes and dispersed ionic conductors.

1. Introduction

During the past decades, ionic liquids (ILs) have attracted a growing interest of research communities in a broad range of fields, from electrochemistry and catalysis to tribology [1–10]. ILs have remarkable properties such as wide electrochemical windows, low volatility or low vapour pressure, which makes them suitable for many applications [11–14]. Moreover, ILs are considered "designer solvents", since their properties can be tuned by changing the combination of anions and cations or combining multiple ILs [15]. One of the most characteristic properties of these dense ionic fluids is their nano-structuration, particularly that they tend to form both polar and apolar nano-domains [16]. This feature explains their capability to solvate almost any kind of solute. It has been reported that mixtures of ILs with solvents of different nature induce significant structural changes in the ionic network inside the molecular structure of these materials. For instance, it is well known that polar solvents such as water tend to form pockets inside the polar nano-regions when mixed with aprotic ILs at low concentrations [17,18]. In contrast, protic ILs integrate well into the hydrogen bond network of water [19]. For amphiphilic solvents like alcohols, this nano-structured solvation mechanism is quite different. The polar heads are placed at the interface of the polar-apolar nano-domains, and the alkyl chains are accommodated in the organic region of the ILs [19,20].

Models developed to describe the behaviour of ILs in mixtures with molecular cosolvents often rely on the Debye–Hückel (DH) theory [21]. However, the DH theory is based on a mean-field approximation for the electrostatic interactions and is valid only for dilute electrolytes. As the ion concentration increases, the molecular structure becomes increasingly more relevant, and more sophisticated theories are needed. A promising approach is based on a pseudo-lattice approximation, known as the Bahe–Varela

* Corresponding author.
E-mail address: luismiguel.varela@usc.es (L.M. Varela).

https://doi.org/10.1016/j.molliq.2022.118955
0167-7322/

(BV) theory [22,23]. This approach describes ionic transport as the hopping of anions and cations between cells with different mobilities associated with molecular cages, whereby the hopping frequencies are the key parameters characterising the underlying physics. A recent modification of this theory introduced the correlations between cells with different mobilities, allowing one to reproduce the conductivities of binary IL-solvent mixtures accurately in the whole concentration range [24].

In this work, we investigate experimentally and with molecular dynamics simulations the structure and dynamic properties of mixtures of ionic liquids with amphiphilic cosolvents. We focus on a mixture of 1-butyl-3-methylimidazolium iodide ([BMIM][I]) with ethanol, which allows us to examine how the solvent nature affects the properties of the mixture by comparing with the earlier work by Sha et al. [25] who studied the same IL in water. Moreover, we also investigate the effect of alkyl chain lengths by considering the same mixtures but using a shorter cation 1-ethyl-3-methylimidazolium ($[EMIM]^+$) instead of $[BMIM]^+$. To analyse the conductivities of these mixtures, we apply the improved BV model [24] and relate it to the microscopic properties such as jumping frequencies.

2. Methods

2.1. Simulations

We have performed bulk MD simulations of mixtures of [BMIM][I] and [EMIM][I] with ethanol for different concentrations using the Gromacs 2019 software [26,27]. A set of 17 and 13 different concentrations of [BMIM][I] and [EMIM][I], respectively, were simulated (see Tab. S1 and S2 in the supplementary information (SI) for the number of molecules and the corresponding simulation box sizes for each concentration) to adequately reproduce the conductivity dome. We chose these ILs to compare with previously reported aqueous mixtures [25]. It has to be mentioned that neat [EMIM][I] is not liquid at room temperature (melting temperature $T_{\text{melting}} = 77\ ^\circ\text{C}$) and is miscible with alcohol only at concentrations up to 80% (according to our experiments). In simulations, we did not observe any signs of crystallisation because the force field we used to simulate [EMIM][I] was optimised for the liquid state. Nevertheless, the simulation results for this IL (particularly at high concentrations) should be taken with caution.

We performed simulations using the OPLS-AA force-field [28] and the parameterization of the employed molecular species used in previous studies [29]. We chose this force-field mainly because, in our experience, it accurately describes the structural properties of these systems at moderate computational costs. However, it is known that this force-field describes the dynamics of ionic species qualitatively well but usually underestimates their diffusion coefficients and polarizable force-fields are needed for more accurate dynamical characterisation [30–32]. Nevertheless, as we will discuss, the obtained results are accurate enough for our purposes.

We first packed the molecules randomly into a simulation box using Packmol [33]. Then, we performed an energy minimisation with the steepest decent algorithm to relax the artificially generated molecular configurations. These initial configurations were used to perform a stabilisation run in the *NpT* ensemble at 1 atm of pressure and room temperature during 10 ns. We finally performed a 20 ns long production run in the same ensemble, recording the atomic positions every 0.4 ps. All the structural properties were calculated from these production runs. For the last two steps, the v-rescale algorithm was used for the thermostat [34], the Parrinello-Rahman for the barostat [35]. The simulation time-step was 2 fs. For the short-time single-particle dynamics analysis, we ran simulations for another 200 ps but with a time step of 1 fs, recording the atomic velocities each simulation step. For the electric current analysis, to avoid problems with fluctuations of the systems' volumes, the final configuration of the previous *NpT* production run was taken as a starting point for a new stabilisation run of 1 ns in the *NVT* ensemble, using the same v-rescale thermostat. This time proved to be sufficient to reach equilibrium, which is because the starting configuration was already stabilised. We then performed another production run for 5 ns, recording the atomic positions every 0.02 ps to calculate conductivities.

2.2. Experimental details

The employed ILs ([EMIM][I] and [BMIM][I]) were purchased from IoLiTec, with a purity higher than 98%. They were dried during 12 h under vacuum and moderate temperature (about 150 °C) to reach water content below 200 ppm. We have not performed any further purification. The ethanol was purchased from PanReac and its purity was higher than 99%.

Mixtures were prepared by weight into a dry box to avoid water absorption from the atmosphere, because these ILs are highly hygroscopic. Concentrations were, in mass percentage of the corresponding IL: 95, 90, 80, 70, 60, 50, 40, 30 and 20% approximately. The measurements were done at room temperature (298.15 K).

Ionic conductivity (σ) was measured using a CRISON GLP31 conductivity meter, which employs an ac voltage of 500 Hz and 0.50 V, with the constant cell calibration parameter $C \simeq 1\ \text{cm}^{-1}$, and the distance between electrodes 3.5 mm. The capacity effect has been evaluated and found to be below the reproducibility of the measured value. Calibration was made weekly with two certified KCl solutions with different concentrations to cover the range of values measured. All measurements were performed using the isothermal method: the sample was immersed into a Julabo F25 thermostatic bath, which controlled the temperature with an uncertainty of $\pm 0.1\ ^\circ\text{C}$, the sample was tempered for at least 15 min before measuring it three consecutive times. The relative experimental uncertainties were less than 0.5% of the measured σ values, with the repeatability better than 3%. The measured conductivities for all the mixtures are presented in Table S3 in the SI.

Due to the corrosive nature of the used ILs, density has been measured at 20 °C following a pycnometric method with a Mettler Toledo balance, with the resulting density uncertainty of $\pm 0.01\ \text{g cm}^{-3}$ and temperature uncertainty $\pm 0.5\ ^\circ\text{C}$. Notice that these data are needed to calculate the molar concentration and the molar conductivity of the mixtures from the weight percentage. The measured values of the densities are presented in Table S4 in the SI.

3. Results and discussion

3.1. Structure

To characterise the structure of the simulated systems, we have calculated the radial distribution functions (RDFs) between different components at different IL molar fractions (Fig. 1). The centre of mass of the cations and anions, and the position of oxygen in alcohol molecules were taken as reference points to calculate distances. Two maxima in the cation–anion RDF suggest two 'adsorption' sites for an I^- anion at a $[BMIM]^+$ cation. As we discuss below (cf. Fig. 2), there are three coordination spots of the anions around cations. However, two of them are at the same distance from the centre of mass of $[BMIM]^+$, hence only two peaks are seen in the RDFs. Interestingly, this structure is preserved throughout the whole range of concentration, which is not the case in systems with water [25].

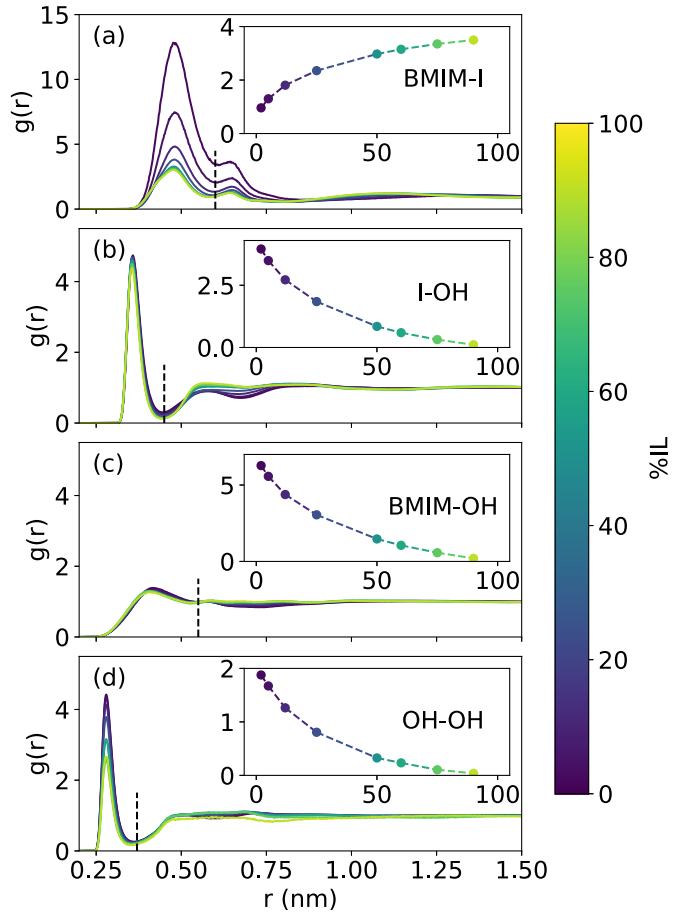

Fig. 1. Radial distribution functions (RDFs) and coordination numbers. (a) Cation–anion, (b) alcohol-anion, (c) alcohol-cation, and (d) alcohol-alcohol RDFs obtained from simulations of [BMIM][I]-alcohol mixtures with different IL molar fractions, indicated by different colours (see the colour bar on the right). The insets show coordination numbers as functions of IL molar fraction. The coordination numbers have been calculated by integrating the RDFs up to the first solvation shell, denoted by vertical black dashed lines in the main figures.

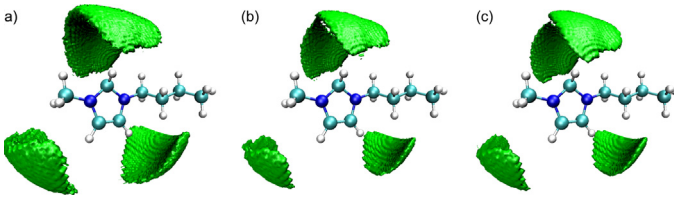

Fig. 2. Spatial distribution functions (SDFs) of $[I]^-$ at $[BMIM]^+$ obtained from molecular dynamics simulations of [BMIM][I] mixed with alcohols for IL molar fractions (a) 0.1, (b) 0.5, and (c) 1. The isosurfaces represent the regions with a more than ten times higher probability of finding an anion than the probability of a homogeneous distribution determined by the anion bulk density.

We also calculated the coordination numbers by integrating the RDFs up to the position of the first solvation shell, determined by the first local minimum

$$CN = 4\pi\rho \int_0^{R_{\min}} r^2 g(r) dr, \tag{1}$$

where ρ is the bulk density of the species to calculate the coordination number. All the coordination numbers vary smoothly with the IL concentration (the insets in Fig. 1), which is what one might expect for a homogeneous mixture. This behaviour is also manifested by solvent–solvent distribution functions (Fig. 1d). Although peaks are present in these distributions, they are small compared to the peaks reported for similar ILs in water [18,25], where one observed the formation of clusters of cosolvent molecules.

Another interesting fact is that there is no change in the preferential adsorption of anions at cations as the IL mole fraction changes, i.e., the RDFs are attenuated as the IL concentration increases but the shape remains the same. Note that the other RDFs do not show any remarkable changes in their shapes and heights of the peaks. This behaviour is again in contrast to water-IL mixtures, where both the shape and the height of the peaks change with the IL concentration. The coordination numbers of alcohols and ions also vary smoothly but decrease with the IL concentration, unlike for the cation–anion (see Fig. S1 in the SI for a snapshot of ethanol molecules from the simulation with 90% of IL, demonstrating that the distribution of alcohol is homogeneous in the system).

We note that these results are in agreement with other results for similar mixtures and hence with the nano-structured solvation paradigm [18–20].

To get more insights into anion-cation coordination, we calculated spatial distribution functions (SDFs) and visualised them with the VMD software [36] (Fig. 2). The SDFs are shown for three different IL mole fractions and demonstrate that the probability of anion-cation coordination does not change appreciably with the addition of solvent. This means that alcohol molecules do not displace anions around a cation, which is again different from aqueous solutions but matches the predictions of the nano-structured solvation paradigm, according to which alcohols are expected to be located in the nano-domain interfaces without forming clusters. This figure also demonstrates the existence of three adsorption sites for iodide, all of them placed towards the C-H bonds in the imidazole ring of the cation. Such adsorption sites have already been reported for this and similar ILs [25,37].

3.2. Ion dynamics

We first analysed velocity autocorrelation functions (VACFs), which were evaluated using the velocity of the centre or mass of each molecular species. The VACF shows a typical behaviour, with a negative region developing for an increasing ion concentration (Fig. 3). This indicates strengthening of the correlations of the molecules with their solvation cages. In other words, the intermolecular interactions and hence caging effects (like rattling motion) of ions and ethanol molecules are enhanced.

We also calculated the Fourier transforms of VACFs (the insets in Fig. 3), which correspond to the vibrational density of states (VDOS, see Ref. [20] for a detailed description). A slight red-shift of the VDOS is observed as the IL concentration decreases (see how the main peak of the VDOS shifts to the left for darker curves), which is due to the attenuation of the intermolecular interactions. This effect is not new and has already been reported for similar mixtures [19,20,25,38]. It is related to the progressive replacement of ionic species by alcohol molecules in the first coordination shell, making the Coulomb interactions weaker. We also note that VACFs profiles varied smoothly with the IL concentration and we did not observe any abrupt changes in the short-time ion dynamics.

The integral of a non-normalised VACF is related to a self-diffusion coefficient through the Green–Kubo relation:

$$D_\pm = \frac{1}{3}\int_0^\infty \left\langle \vec{v}_\pm(0)\,\vec{v}_\pm(t)\right\rangle dt, \tag{2}$$

where $\vec{v}_\pm$ is the velocity of $\pm$ ions and $\langle\cdots\rangle$ denotes thermal averaging. Although the representation of the VACFs in Fig. 3 is done up to 0.8 ps, to calculate their integrals we use the full set of data that goes up to 100 ps so the long-time correlations, which are known to be relevant in these dense ionic fluids [39,40], are taken into

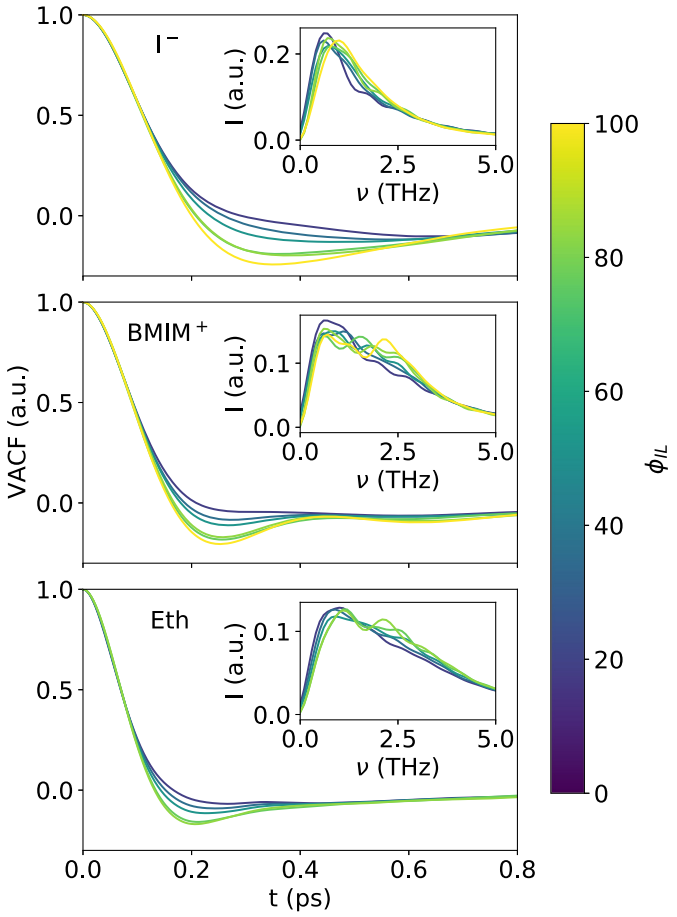

Fig. 3. Velocity autocorrelation functions (VACFs) and vibrational density of states (VDOS). Normalised VACFs obtained by molecular dynamics simulations are shown for different molecular species and for different IL volume fractions, as indicated by different colours (see the colour bar on the right). The insets show the corresponding VDOSs. Note that the colour code is set according to the volume fraction of IL (ϕ_{IL}), which is more convenient for further comparison with theoretical predictions (see Table S1 and S2 in the SI for the correspondence between molar and volume fractions).

account. The diffusion coefficients can also be calculated from the linear fit of the mean squared displacements (MSDs) of the ions in the diffusive regime:

$$D_{\pm} = \frac{1}{6}\lim_{t\to\infty}\frac{d}{dt}\left\langle\left|\vec{r}_{\pm}(t) - \vec{r}_{\pm}(0)\right|^2\right\rangle. \tag{3}$$

Although both equations should provide the same value for the diffusion coefficients, we nevertheless observe small discrepancies (Fig. 4). It is interesting to note that the values obtained by integrating the VACFs (Eq. (2)) are slightly higher than those obtained with the fit of the MSDs. To calculate the diffusion coefficients via MSDs accurately, long simulations are required to guarantee that the ionic species enter in the diffusive regime, especially for the most concentrated systems. Therefore, the slope of the fit is lower than in the long-time normal diffusive regime, and so are the so calculated diffusion coefficients (Fig. S2 in the SI). We note that these differences exist due to the complex nature of ionic compounds, which translates into a slow dynamics.

3.3. Conductivities

We first used the Nernst–Einstein equation,

$$\sigma_{N-E} = \frac{Ne^2}{Vk_BT}(D_+ + D_-), \tag{4}$$

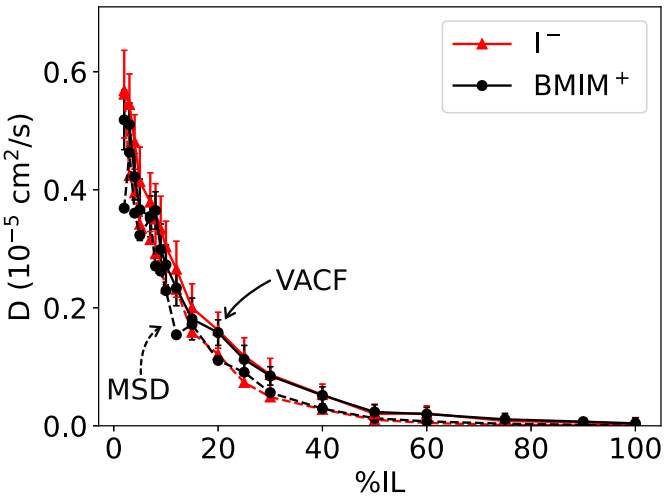

Fig. 4. Self-diffusion coefficients of ions. The diffusion coefficients have been calculated using Eq. (3) (dashed lines) and Eq. (2). (solid lines).

to compute the conductivity from the diffusion coefficients calculated via MSD and VACFs. However, the Nernst–Einstein approximation does not take into account anion-cation correlations, which can be relevant in mixtures of ILs with molecular cosolvents [41]. To take into account these correlations, we calculated the ionic conductivity from the ionic current autocorrelation function using the Green–Kubo relation:

$$\sigma_{G-K} = \frac{1}{3Vk_BT}\int_0^{\infty}\left\langle\vec{j}(0)\vec{j}(t)\right\rangle dt, \tag{5}$$

where $\vec{j}(t)$ is the total current at time t,

$$\vec{j}(t) = \sum_{i=1}^{N} q_i\vec{v_i}(t). \tag{6}$$

Here the sum runs over all atoms in the system, and q_i and $\vec{v_i}$ are their charge and velocity.

To evaluate the integral in Eq. (5), we first calculated this integral to a finite time t, obtaining $I(t)$. For all concentrations, we found a relatively good convergence of $I(t)$ for times above 50 ps. We then averaged $I(t)$ in the interval between 50 ps to 100 ps to calculate the conductivity (Fig. S3 in the SI). In this way, we also obtained the standard deviations of the fluctuations and an estimation of the uncertainty.

In Fig. 5, we show the conductivities calculated using the Nernst–Einstein and Green–Kubo formalisms. Similarly to the diffusion coefficients (Fig. 4), the conductivities calculated with the fits of MSDs are slightly lower than those obtained with the integral of VACFs. Both methods predict higher conductivities than calculated with the Green–Kubo relation. This is because anion-cation current correlations, which are present only in the latter approach, reduce the conductivity compared with the conductivities calculated only with the self-diffusion of anions and cations. Apart from these differences, all the methods show a maximum of the conductivity at approximately the same IL concentration (ca. 15% of IL molar fraction). The existence of this maximum is due to the combination of two effects. On the one hand, the number of charge carriers increases as the IL concentration increases, increasing the conductivity. On the other hand, the ion mobility decreases due to the increased crowding (Fig. 4). This reasoning implies that there is at least one maximum in the conductivity. While this phenomenon has already been reported in numerous experimental and computational studies [25,42–44], our results show that the

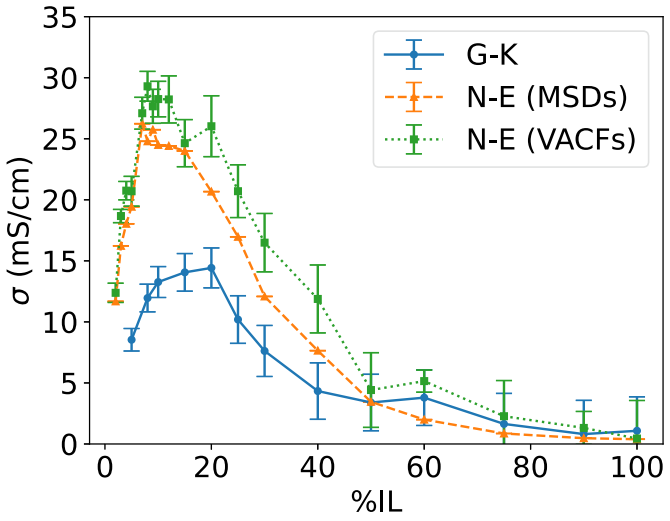

Fig. 5. Ionic conductivities calculated using the Nernst–Einstein approximation with the diffusion coefficients obtained from MSDs and VACFs and by using the Green–Kubo equation for the [BMIM][I]-alcohol mixtures.

effect of ion correlations is most relevant at concentrations close to the conductivity maximum.

3.4. Comparison with experiments

Given the results obtained by the three methods, we used the conductivities calculated with the Green–Kubo approach to compare with our experimental results. The comparison is shown in Fig. 6 for two IL mixtures. For both ILs, the computed conductivity underestimates the experimental results in the whole concentration range. This is likely because we employed a non-polarizable force-field in our simulations, which is known to predict slower dynamics and thus lower conductivities [31]. Borodin [45] investigated the effect of polarization on ion density and diffusion. This author used [EMIM][BF_4] IL, i.e., a cation of the same family as in our work, and revealed that turning off the polarization increases the free volume in the system but induces structural changes that slow down the ionic dynamics.

Note that the conductivity maxima are shifted towards lower IL volume fractions. This shift is also likely related to slower dynamics due to the non-polarizable force field, which reduces the ion mobility stronger for the increasing ion concentration.

Despite these differences, the simulation results nevertheless reproduce the trends of the conductivity dome well. This suggests that for mixtures of IL and molecular cosolvents, one can use computationally less expansive non-polarizable force fields to understand the underlying physics qualitatively or compare to other systems.

3.5. Fitting to the pseudo-lattice random-alloy model

Within the pseudo-lattice random-alloy model, the transport of ionic species is described by jumps between neighbouring cells, defined by the solvation cages of the mobile species [24]. The jumps are performed with an average jumping frequency that depends on the initial and final cells, which are classified into two different types: low mobility α-cells and β-cells with higher mobility. The former are associated with regions of high ion concentrations and the latter are the regions with high solvent concentrations. This approach leads to the following simple equation for ionic conductivity [24]:

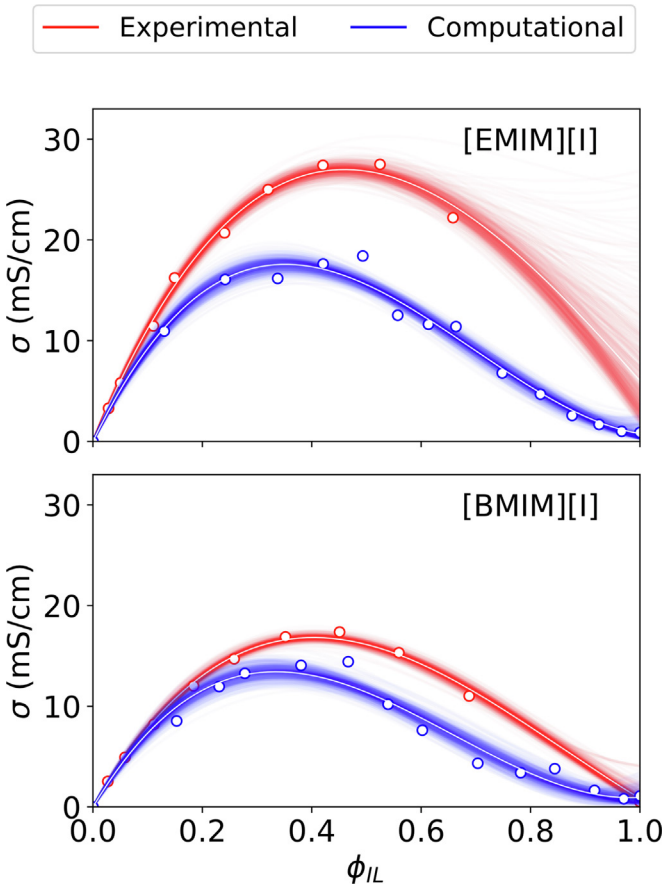

Fig. 6. Comparison of the simulation and experimental results for two ionic liquids. The plots show the Bayesian regression of the experimental and computational results of the conductivities to the pseudo-lattice random-alloy model, Eq. (7), as a function of IL volume fraction. The white lines inside the coloured regions represent the most probable fit. The coloured regions are the result of the superposition of randomly chosen 1% of all the curves estimated by the regression.

$$\sigma(\phi) = \sigma_{IL}\left[\phi(1-\phi)\tilde{\nu}_B + \phi^2 + \phi^2(1-\phi)\Delta\nu\right], \tag{7}$$

where σ_{IL} is the conductivity of the pure IL phase and ϕ is the IL volume fraction. Parameters $\tilde{\nu}_B$ and $\Delta\nu$ are related to the jumping frequencies between high and low mobility regions (c.f. Eq. (10))

$$\tilde{\nu}_B = \frac{\nu_{\beta\beta}}{\nu_{\alpha\alpha}} \tag{8}$$

and

$$\Delta\nu = \frac{\left(\nu_{\alpha\beta} + \nu_{\beta\alpha}\right) - \left(\nu_{\alpha\alpha} + \nu_{\beta\beta}\right)}{\nu_{\alpha\alpha}}, \tag{9}$$

where $\nu_{\alpha\gamma}$ is the jumping rate between α and γ cells. Therefore, $\tilde{\nu}_B$ represents the jumping rate between β cells and $\Delta\nu$ the difference in jumping rates between similar and dissimilar cells, with both quantities normalised by the jumping rate between α cells (see Fig. S4 on the SI for a schematic of different jumping frequencies).

The reader is referred to Ref. [24] for a more detailed description of the theoretical formalism. We note that using jumping frequencies between two types of cells allows one to characterize various ionic systems. For instance, the model can accurately describe experimental and simulation results with and without polarization; indeed, the differences among them will be incorporated in the jumping frequencies of the individual ionic species.

To evaluate how our experimental and computational results fit to this theory, we performed their Bayesian regression [46] to Eq. (7) using a Markov chain Monte Carlo estimator [47]. Using this

method instead of the standard least squares regression allowed us to obtain the probability distributions of the model parameters. We also supplied additional information on the model parameters; namely, we assumed positive values for the conductivity and restricted the volume fraction at the conductivity maximum to the interval between zero and one. Fig. 6 shows some of the estimated curves compatible with the model; the most probable results are shown by white lines inside the coloured regions.

The obtained values of the model parameters and conductivity maxima are summarised in Table 1. For both ILs, the fit of the computational results predicts the maximum of conductivity at lower IL concentration than obtained by experiments (for [EMIM][I], $\phi_{IL} \approx 0.46$ in the experiments and $\phi_{IL} \approx 0.35$ in the simulations; for [BMIM][I], $\phi_{IL} \approx 0.4$ in the experiments and $\phi_{IL} \approx 0.34$ in the simulations). As discussed, this is likely because we used a non-polarizable force field which tends to underestimate dynamics.

The Bayesian regression also shows how the lack of experimental data at high IL volume fractions (due to the immiscibility of both compounds) affects the model predictions in this region, leading to a wide statistical distribution of the predicted conductivity values for pure [EMIM][I]. This wide distribution translates into a larger uncertainty compared with [BMIM][I] (Table 1).

Comparing both systems, it is clear that the conductivity takes higher values for mixtures with [EMIM][I], which is a consequence of the lower mass and higher mobility of the cation. Similar results have been reported by Chaban et al. for mixtures of [BMIM][BF_4] and [EMIM][BF_4] with acetonitrile [44] and by Rilo et al. for mixtures with ethanol [48]. This is also similar to changing the size of the solvent: for smaller solvents, such as methanol, the ionic mobility is higher than for larger similar molecules, for example, butanol [42].

It is noteworthy that the maxima of the conductivity take place at roughly the same IL volume fraction for both mixtures (albeit different in simulations and experiments: ≈ 0.34 and ≈ 0.43, respectively). This 'invariance' of the maximum position with respect to the cation alkyl chain length has also been observed for mixtures of [BMIM][I] and [EMIM][I] with acetonitrile [44]. A similar phenomenon has been reported for mixtures of [EMIM] alkyl-sulphate with water and ethanol, where the conductivity maximum did not change appreciably with changing the alkyl chain length of the anion [24]. This effect can be rationalised by assuming that conductivity is uniquely determined by the fraction of free ions in the solution, i.e., the ions surrounded by solvent molecules and not associated with other ions. This assumption means that the conductivity maximum for larger ions must correspond to the same fraction of free ions. However, more solvent molecules are needed to isolate larger ions, implying that the solvent concentration at the conductivity maximum must increase. Still, the volume fraction should remain roughly the same due to a larger volume taken up by the ions (see an article by Nordness and Brennecke [49] for a more detailed description of this effect and its application to multiple binary mixtures of ILs and molecular cosolvents).

We close this subsection by pointing out an excellent fit that the random-alloy pseudo-lattice model provides for experimental and simulation data. This suggests it as a tool to predict the shape of the conductivity dome from a few simulations or experimental data and, in particular, to find the optimal concentration maximizing the conductivity.

3.6. Jumping frequencies

An important conclusion that can be drawn from Fig. 6 is that the pseudo-lattice random-alloy model, Eq. (7), fits well all our conductivity data sets. This model describes the behaviour of a macroscopic quantity (conductivity) based on microscopic quantities, namely, ion jumping frequencies between different cells, which can be identified as ionic solvation shells. We recall that the model distinguishes two different types of cells, depending on the local environment of an ion. In principle, one could calculate these frequencies by analysing the structure of the solvation shell and the time an ion needs to leave it. However, a criterion to identify different cell types in simulations is not straightforward. Thus, instead of analysing jumping between different cells, we consider an average frequency

$$\bar{\nu}(\phi) = \sum_{\alpha,\beta} P_{\alpha\beta}(\phi)\nu_{\alpha\beta}, \tag{10}$$

where $P_{\alpha\beta}(\phi)$ is the concentration-dependent probability to find two neighbouring cells α and β. To calculate $\bar{\nu}$ from simulations, we wrote a Python script using MDAnalysis [50,51], which computes the average time it takes for an ion to move a distance of 5 Å(the size of the solvation shell). The obtained values are shown by symbols in Fig. 7. As one may expect, the average jumping frequency decreases with increasing the IL volume fraction. This decrease is consistent with the decrease of the diffusion coefficients (Fig. 4).

The average frequency and conductivity are related by [24]

$$\sigma = a^2 q^2 \rho_{\text{free}} \bar{\nu}/k_B T, \tag{11}$$

where ρ_{free} is the density of free charge carriers and q is their charge. One easily finds (c.f. Eq. (7)),

$$\bar{\nu}(\phi) = \nu_{\alpha\alpha}[\phi + (1-\phi)\tilde{\nu}_B + \phi(1-\phi)\Delta\nu], \tag{12}$$

where $\nu_{\alpha\alpha} = k_B T \sigma_{IL}/(a^2 q^2 \rho_{\text{free}})$ is the jumping frequency between α cells. Since ρ_{free} is not known, we used $\nu_{\alpha\alpha}$ as a fitting parameter, and $\tilde{\nu}$ and $\Delta\nu$ from Table 1, to calculate the average frequency from the conductivity data. The results are represented as solid lines in Fig. 7 and agree well with the values computed directly from simulations. This agreement implies the consistency of the relation between microscopic jumping frequencies and macroscopic conductivity (Eq. (11)), which suggests that the microscopic picture assumed by the pseudo-lattice theory is compatible with the simulation results.

Table 1
The most probable values of the pseudo-lattice random-alloy model fit to the computational and experimental results for mixtures of [EMIM][I] and [BMIM][I] with ethanol.

	[EMIM][I]		[BMIM][I]	
	Comp.	Exp.	Comp.	Exp.
σ_{IL} (mS/cm)	0.77±0.56	6.0±4.2	0.94±0.62	0.85±0.63
$\tilde{\nu}_B$	210±120	30±16	140±89	145±64
$\Delta\nu$	−190±100	−12.0±6.1	−138±82	−90±40
$\phi(\sigma_{max})$	0.3520±0.0092	0.460±0.016	0.335±0.013	0.4036±0.0091
σ_{max} (mS/cm)	17.58±0.55	27.00±0.51	13.44±0.61	16.84±0.25

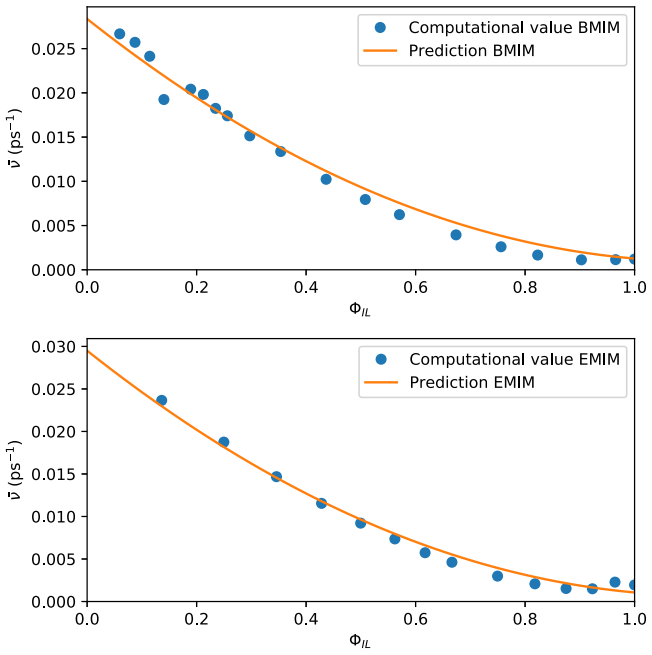

Fig. 7. Average jumping frequency $\bar{\nu}$ as a function of the ion volume fraction. The symbols show the results obtained by computing $\bar{\nu}$ directly from simulations. The solid lines show the results obtained by using Eq. (12) as described in the text. The top plot is for [BMIM][I] and the bottom plot for [EMIM][I] mixtures.

4. Conclusions

We have studied the structural and dynamic properties of [EMIM][I] and [BMIM][I] in alcohol using MD simulations and experimental measurements of ionic conductivities. The structural analysis showed the absence of alcohol clusters in these mixtures, but the relatively homogeneous distribution of all species, in agreement with the nano-structured solvation paradigm [19,18,20]. The coordination of anions around cations was not altered by increasing the alcohol concentration (Fig. 2). These results are different compared with the behaviour of the same ionic liquids in water, where water tends to form pockets inside polar nano-regions of the ionic liquid [17,18]. We note that these differences with aqueous electrolytes are the main reason for the drastic differences in other quantities, particularly transport properties.

We analysed the short-time single-particle dynamics with velocity autocorrelation functions (VACFs) and vibrational density of states (VDOSs) (Fig. 3). Caging of all species became more pronounced but varied smoothly as the ion concentration increased, indicating stronger interactions in the molecular surroundings of all species.

We used VACFs to compute ion's diffusion coefficients and hence the conductivity via the Nernst–Einstein equation (Eq. (4)). This method slightly overestimated the conductivities compared to the ones obtained from the long-time dynamics through mean square displacements (MSDs) and from the current autocorrelation functions using the Green–Kubo relation, Eq. (5) (Fig. 5). The conductivities calculated with the latter method showed a reasonably good agreement with our experimental results (Fig. 6). The simulation results reproduced well the conductivity dome, although they slightly underestimated the measured values.

The pseudo-lattice random-alloy model (Eq. (7)) fitted the experimental and simulations results for the conductivities well. This model describes ion transport as jumps between cells with different mobilities. Using our simulation data, we computed directly the jumping frequency averaged over different types of cells and found a good agreement with the average frequency obtained from fitting the simulation conductivity data (Fig. 7). This agreement suggests that the microscopic picture of ion transport assumed by the pseudo-lattice model is consistent with simulations. While this model has been developed to describe the dependence of conductivity on IL concentration, one can combine it with the Arrhenius law to investigate the temperature dependence, as outlined in Ref. [24]. One can also employ it to predict the concentration at which the conductivity reaches a maximum by performing only a few measurements or simulations, thus reducing the overall computational/experimental costs.

In future work, it will be interesting to identify different cell types in simulations and compute the corresponding jumping frequencies, which would allow the computation of conductivities in the whole concentration range based solely on microscopic frequency data.

CRediT authorship contribution statement

J. Manuel Otero-Mato: Conceptualization, Methodology, Software, Validation, Formal Analysis, Investigation, Data Curation, Writing – Original Draft, Writing – Review & Editing, Visualization. **Hadrián Montes-Campos:** Conceptualization, Methodology, Software, Validation, Formal Analysis, Investigation, Data Curation, Writing – Original Draft, Writing – Review & Editing, Visualization. **Víctor Gómez-González:** Conceptualization, Methodology, Validation, Formal Analysis, Investigation, Data Curation. **Martín Montoto:** Methodology, Investigation, Data Curation. **Oscar Cabeza:** Methodology, Investigation, Data Curation, Writing – Original Draft, Writing – Review & Editing, Funding acquisition. **Svyatoslav Kondrat:** Conceptualization, Methodology, Validation, Formal Analysis, Investigation, Writing – Original Draft, Writing – Review & Editing. **Luis M. Varela:** Conceptualization, Methodology, Validation, Formal Analysis, Investigation, Writing – Original Draft, Writing – Review & Editing, Supervision, Project administration, Funding acquisition.

Declaration of Competing Interest

The authors declare that they have no known competing financial interests or personal relationships that could have appeared to influence the work reported in this paper.

Acknowledgements

The financial support of the Spanish Ministry of Economy and Competitiveness (Projects MAT2017-89239-C2-1-P and MAT2017-89239- C2-2-P) is gratefully acknowledged. Moreover, this work was funded by the Xunta de Galicia (ED431D 2017/06, ED431E 2018/08, GRC ED431C 2016/001 and GRC ED431C 2020/10). All these research projects were partially supported by FEDER. The help of the technician M. C. V. from UDC for some of the measurements presented is also acknowledged. H. M-C. and J. M. O-M. thank the Spanish Ministry of Education for their FPU grant, and H. M-C. thanks the USC for his "Convocatoria de Recualificación do Sistema Universitario Español-Margarita Salas" postdoc grant under the "Plan de Recuperación Transformación" program funded by the Spanish Ministry of Universities with European Union's NextGenerationEU funds.

Appendix A. Supplementary material

Supplementary data associated with this article can be found, in the online version, at https://doi.org/10.1016/j.molliq.2022.118955.

References

[1] J. D. Holbrey, W. M. Reichert, S. K. Spear, R. P. Swatloski, M. B. Turner, A. E. Visser, Ionic Liquids as Green Solvents: Progress and Prospects, in: ACS Symposium Series, vol. 856, 2003.
[2] H. Zhao, S.V. Malhotra, Applications of Ionic Liquids in Organic Synthesis, Aldrichimica Acta. (2002).
[3] R.D. Rogers, K.R. Seddon, Ionic Liquids as Green Solvents: Progress and Prospects, American Chemical Society, 2003.
[4] N.V. Plechkova, K.R. Seddon, Applications of Ionic Liquids in the Chemical Industry, Chem. Soc. Rev. 37 (1) (2008) 123–150.
[5] C. Reichardt, T. Welton, Solvents and Solvent Effects in Organic Chemistry, John Wiley & Sons, 2011.
[6] P. Wasserscheid, T. Welton, Ionic Liquids in Synthesis, John Wiley & Sons, 2008.
[7] I. Minami, Ionic Liquids in Tribology, Molecules 14 (6) (2009) 2286–2305.
[8] M. Galiński, A. Lewandowski, I. Stepniak, Ionic Liquids as Electrolytes, Electrochim. Acta 51 (2006) 5567–5580.
[9] A. Matic, B. Scrosati, Ionic Liquids for Energy Applications, MRS Bullet 38 (07) (2013) 533–537, ISSN 1938–1425.
[10] M. Armand, F. Endres, D.R. MacFarlane, H. Ohno, B. Scrosati, Ionic-Liquid Materials for the Electrochemical Challenges of the Future, Nat. Mater. 8 (2009) 621–629.
[11] S. Zhang, N. Sun, X. He, X. Lu, X. Zhang, Physical Properties of Ionic Liquids: Database and Evaluation, J. Phys. Chem. Ref. Data 35 (4) (2006) 1475–1517.
[12] M. Freemantle, An Introduction to Ionic Liquids, RSC Publishing, 2009.
[13] P. Wasserscheid, T. Welton, Ionic Liquids in Synthesis, Wiley Online Library, 2003.
[14] S. Zhang, X. Lu, Q. Zhou, X. Li, X. Zhang, S. Li, Ionic Liquids: Physicochemical Properties, Elsevier, 2009.
[15] R.D. Rogers, K.R. Seddon, Ionic Liquids- Solvents of the Future?, Science 302 (5646) (2003) 792–793
[16] A.A.H. Pádua, M.F.C. Gomes, J.N.A. Canongia-Lopes, Molecular Solutes in Ionic Liquids: A Structural Perspective, Acc. Chem. Res. 40 (11) (2007) 1087–1096.
[17] S. Feng, G.A. Voth, Molecular Dynamics Simulations of Imidazolium-Based Ionic Liquid/Water Mixtures: Alkyl Side Chain Length and Anion Effects, Fluid Phase Equilib. 294 (1–2) (2010) 148–156.
[18] T. Mendez-Morales, J. Carrete, O. Cabeza, L.J. Gallego, L.M. Varela, Molecular Dynamics Simulation of the Structure and Dynamics of Water- 1-Alkyl-3-Methylimidazolium Ionic Liquid Mixtures, J. Phys. Chem. B 115 (21) (2011) 6995–7008.
[19] B. Docampo-Álvarez, V. Gómez-González, T. Méndez-Morales, J. Carrete, J.R. Rodríguez, Ó. Cabeza, L.J. Gallego, L.M. Varela, Mixtures of Protic Ionic Liquids and Molecular Cosolvents: A Molecular Dynamics Simulation, J. Chem. Phys. 140 (21) (2014) 214502.
[20] H. Montes-Campos, J.M. Otero-Mato, T. Méndez-Morales, E. López-Lago, O. Russina, O. Cabeza, L.J. Gallego, L.M. Varela, Nanostructured Solvation in Mixtures of Protic Ionic Liquids and Long-Chained Alcohols, J. Chem. Phys. 146 (12) (2017) 124503, ISSN 0021-9606.
[21] P. Debye, E. Hückel, I. Zur Theorie der Elektrolyte, Das Grenzgesetz Für Die Elektrische Leitfähigkeit, Phys. Z. 24 (1923) 305–325.
[22] L.W. Bahe, Structure in Concentrated Solutions of Electrolytes. Field-Dielectric-Gradient Forces and Energies, J. Phys. Chem. 76 (7) (1972) 1062–1071.
[23] L.M. Varela, M. Garcia, F. Sarmiento, D. Attwood, V. Mosquera, Pseudolattice Theory of Strong Electrolyte Solutions, J. Chem. Phys. 107 (16) (1997) 6415–6419.
[24] H. Montes-Campos, S. Kondrat, E. Rilo, O. Cabeza, L.M. Varela, Random-Alloy Model for the Conductivity of Ionic Liquid-Solvent Mixtures, J. Phys. Chem. C 124 (22) (2020) 11754–11759.
[25] M. Sha, H. Dong, F. Luo, Z. Tang, G. Zhu, G. Wu, Dilute or Concentrated Electrolyte Solutions? Insight from Ionic Liquid/Water Electrolytes, J. Phys. Chem. Lett. 6 (18) (2015) 3713–3720.
[26] M.J. Abraham, T. Murtola, R. Schulz, S. Páll, J.C. Smith, B. Hess, E. Lindahl, GROMACS: High Performance Molecular Simulations through Multi-Level Parallelism from Laptops to Supercomputers, SoftwareX 1 (2015) 19–25.
[27] B. Hess, C. Kutzner, D.V.D. Spoel, E. Lindahl, GROMACS 4: Algorithms for Highly Efficient, Load-Balanced, and Scalable Molecular Simulation, J. Chem. Theory Comput. 4 (3) (2008) 435–447.
[28] W.L. Jorgensen, D.S. Maxwell, J. Tirado-Rives, Development and Testing of the OPLS All-Atom Force Field on Conformational Energetics and Properties of Organic Liquids, J. Am. Chem. Soc. 118 (45) (1996) 11225–11236.
[29] B. Docampo-Álvarez, V. Gómez-González, T. Méndez-Morales, J.R. Rodríguez, E. López-Lago, O. Cabeza, L.J. Gallego, L.M. Varela, Molecular Dynamics Simulations of Mixtures of Protic and Aprotic Ionic Liquids, Phys. Chem. Chem. Phys. 18 (34) (2016) 23932–23943.
[30] O. Borodin, Molecular Dynamics Simulations of Ionic Liquids: Influence of Polarization on IL Structure and Ion Transport, Mater. Res. Soc. Proc. 1082 (2008), Q06–04.
[31] V. Lesch, H. Montes-Campos, T. Méndez-Morales, L.J. Gallego, A. Heuer, C. Schröder, L.M. Varela, Molecular Dynamics Analysis of the Effect of Electronic Polarization on the Structure and Single-Particle Dynamics of Mixtures of Ionic Liquids and Lithium Salts, J. Chem. Phys. 145 (20) (2016) 204507.
[32] T. Yan, C.J. Burnham, M.G.D. Pópolo, G.A. Voth, Molecular Dynamics Simulation of Ionic Liquids: The Effect of Electronic Polarizability, J. Phys. Chem. B 108 (32) (2004) 11877–11881.
[33] L. Martínez, R. Andrade, E.G. Birgin, J.M. Martínez, PACKMOL: A Package for Building Initial Configurations for Molecular Dynamics Simulations, J. Comput. Chem. 30 (13) (2009) 2157–2164.
[34] G. Bussi, D. Donadio, M. Parrinello, Canonical Sampling through Velocity Rescaling, J. Chem. Phys. 126 (1) (2007) 014101.
[35] M. Parrinello, A. Rahman, Polymorphic Transitions in Single Crystals: A New Molecular Dynamics Method, J. Appl. Phys. 52 (12) (1981) 7182–7190.
[36] W. Humphrey, A. Dalke, K. Schulten, VMD: Visual Molecular Dynamics, J. Mol. Graphics 14 (1) (1996) 33–38.
[37] B. Docampo-Álvarez, V. Gómez-González, T. Méndez-Morales, J.R. Rodríguez, O. Cabeza, M. Turmine, L.J. Gallego, L.M. Varela, The Effect of Alkyl Chain Length on the Structure and Thermodynamics of Protic–Aprotic Ionic Liquid Mixtures: A Molecular Dynamics Study, Phys. Chem. Chem. Phys. 20 (15) (2018) 9938–9949.
[38] T. Méndez-Morales, J. Carrete, O. Cabeza, L.J. Gallego, L.M. Varela, Molecular Dynamics Simulations of the Structural and Thermodynamic Properties of Imidazolium-Based Ionic Liquid Mixtures, J. Phys. Chem. B 115 (38) (2011) 11170–11182.
[39] C. Schröder, M. Haberler, O. Steinhauser, On the computation and contribution of conductivity in molecular ionic liquids, J. Chem. Phys. 128 (13) (2008) 134501.
[40] C. Schröder, O. Steinhauser, On the dielectric conductivity of molecular ionic liquids, J. Chem. Phys. 131 (11) (2009) 114504.
[41] J.G. McDaniel, C.Y. Son, Ion Correlation and Collective Dynamics in BMIM/BF4-based Organic Electrolytes: From Dilute Solutions to the Ionic Liquid Limit, J. Phys. Chem. B 122 (28) (2018) 7154–7169.
[42] M.W. Thompson, R. Matsumoto, R.L. Sacci, N.C. Sanders, P.T. Cummings, Scalable Screening of Soft Matter: A Case Study of Mixtures of Ionic Liquids and Organic Solvents, J. Phys. Chem. B 123 (6) (2019) 1340–1347.
[43] E. Rilo, J. Vila, S. García-Garabal, L.M. Varela, O. Cabeza, Electrical Conductivity of Seven Binary Systems Containing 1-Ethyl-3-Methyl Imidazolium Alkyl Sulfate Ionic Liquids with Water or Ethanol at Four Temperatures, J. Phys. Chem. B 117 (5) (2013) 1411–1418.
[44] V.V. Chaban, I.V. Voroshylova, O.N. Kalugin, O.V. Prezhdo, Acetonitrile Boosts Conductivity of Imidazolium Ionic Liquids, J. Phys. Chem. B 116 (26) (2012) 7719–7727, ISSN 1520–6106.
[45] O. Borodin, Polarizable force field development and molecular dynamics simulations of ionic liquids, J. Phys. Chem. B 113 (33) (2009) 11463–11478.
[46] B. Gep, G. Tiao, Bayesian Inference in Statistical Analysis, Reading: Addison-Wesley, 2011.
[47] J. Salvatier, T.V. Wiecki, C. Fonnesbeck, Probabilistic Programming in Python Using PyMC3, PeerJ Comput. Sci. 2 (2016) e55, ISSN 2376-5992.
[48] E. Rilo, J. Vila, M. Garcia, L.M. Varela, O. Cabeza, Viscosity and electrical conductivity of binary mixtures of CnMIM-BF4 with ethanol at 288 K, 298 K, 308 K, and 318 K, J. Chem. Eng. Data 55 (11) (2010) 5156–5163.
[49] O. Nordness, J.F. Brennecke, Ion dissociation in ionic liquids and ionic liquid solutions, Chem. Rev. 120 (23) (2020) 12873–12902.
[50] N. Michaud-Agrawal, E.J. Denning, T.B. Woolf, O. Beckstein, MDAnalysis: A Toolkit for the Analysis of Molecular Dynamics Simulations, J. Comput. Chem. 32 (10) (2011) 2319–2327.
[51] R.J. Gowers, M. Linke, J. Barnoud, T.J.E. Reddy, M.N. Melo, S.L. Seyler, J. DomaÅski, D.L. Dotson, S. Buchoux, I.M. Kenney, Oliver Beckstein, MDAnalysis: A Python Package for the Rapid Analysis of Molecular Dynamics Simulations, in: S. Benthall, Scott Rostrup (Eds.), Proceedings of the 15th Python in Science Conference, 2016, pp. 98–105.